

RMS Delay and Coherence Bandwidth Measurements in Indoor Radio Channels in the UHF Band

Mercedes Sánchez Varela and Manuel García Sánchez, *Member, IEEE*

Abstract—A study of time dispersion in different indoor line-of-sight radio channels in the 492–862 MHz band is presented in this paper. A combined method to filter the noise in the measured impulse response is described. The effect of frequency windowing on the impulse responses and the root mean square (rms) delay spread is also investigated. It has been found that, in general, the use of windows with lower side-lobe levels yields larger values of the rms delay spread. The relation between the mean delay and the rms delay spread has also been studied for copolar and crosspolar channels. The dependence of the coherence bandwidth on the rms delay spread has been considered, and an inverse relation has been tested for both components.

Index Terms—Communication channels, communication systems, parameter estimation, UHF measurements, UHF radio propagation.

I. INTRODUCTION

THE dramatic increase of the number of digital radio communication systems within buildings has demanded wide band characterization of indoor radio channels. Signal time dispersion is one of the main study issues because it limits the maximum symbol rate that can be used without intersymbol interference [1]. The impulse response (IR) of the radio channel and other parameters, as the mean delay (τ_{mean}) and the root mean square (rms) delay spread (τ_{rms}) [2], [3], are frequently used to characterize time dispersion of the channel. The coherence bandwidth (B_c), a parameter closely related with τ_{rms} , is also used to describe frequency selectivity in the radio channel.

Previous works have investigated the relation between B_c and τ_{rms} , and different solutions have been found for outdoor environments [1]–[6]. But at present, few experimental results exist that describe the relation between B_c and τ_{rms} in indoor environments. In this paper, an experimental study on the relation between these parameters inside buildings is presented. The results are based on wide-band measurements taken in three different indoor environments with a frequency swept radio channel sounder. The sounder, based on a vector network analyzer (VNA), has been used to measure the frequency response of the radio channel in the 470–862 MHz frequency band. From the frequency response, both the B_c and the IR are obtained. The effect of the frequency windowing on the IR shape, τ_{mean} , and τ_{rms} is analyzed. A method to filter the noise

out from the IR is also presented. The parameters τ_{mean} and τ_{rms} are obtained from this filtered IR.

A linear relation between τ_{mean} and τ_{rms} and an inverse relation between τ_{rms} and B_c are investigated for line-of-sight (LoS) situations in the three environments considered, both for copolar and crosspolar components. The values of the least mean square (LMS) error and the 90% confidence interval are given for the different fits.

II. MEASUREMENT SETUP AND THEORETICAL FUNDAMENTALS

An HP 8510C VNA was used to obtain the frequency response of the radio channel in the 470–862 MHz frequency band [7]. The measurement setup is shown in Fig. 1. The copolar component was measured with two vertical 3-dBi omnidirectional dipole antennas connected to the input and output ports of the VNA and placed on the top of a 1-m-height tripod. To measure the crosspolar component, the vertical dipole at the receiver was replaced by a 5-dBi omnidirectional antenna consisting of two orthogonal folded dipoles. This antenna was horizontally polarized.

The measurement system output is the frequency response of the devices connected between its two ports, including the channel, antennas, cables, amplifiers, and frequency response of the VNA itself. To compensate the effect of the system on the measurements, a calibration was carried out before the radio channel measurements. With this purpose, the antennas were removed so that the transmitter output was directly connected to the receiver input, its frequency response $H(f)_{\text{system}}$ being measured. This result was automatically subtracted from the subsequent channel measurements, thus reducing the effect of the system on the measurement

$$H(f, t)_{\text{channel}} = \frac{H(f, t)_{\text{measured}}}{H(f)_{\text{system}}}. \quad (1)$$

If the channel is linear, the IR can be calculated from the frequency response using the inverse Fourier transform [8]

$$h(\tau, t) = \int_{-\infty}^{\infty} H(f, t) e^{j2\pi ft} df. \quad (2)$$

However, since the measurements were performed over a limited frequency band, there was a windowing effect on the results

$$\begin{aligned} h(\tau, t)_{\text{estimated}} &= \int_{f_{\min}}^{f_{\max}} H(f, t) e^{j2\pi ft} df \\ &= \int_{-\infty}^{\infty} H_{\text{channel}}(f, t) \cdot H_{\text{window}}(f) e^{j2\pi ft} df. \end{aligned} \quad (3)$$

Manuscript received June 30, 1999; revised July 25, 2000. This work was supported by the Spanish Comisión Interministerial de Ciencia y Tecnología (CICYT) under Project TIC97-1129-C04-03.

The authors are with the Departamento De Tecnoloxias Das Comunicacions, E.T.S.E. Telecomunicacións, Universidade de Vigo, Vigo 36200, Spain (e-mail: mgarcia@tsc.uvigo.es).

Publisher Item Identifier S 0018-9545(01)03073-0.

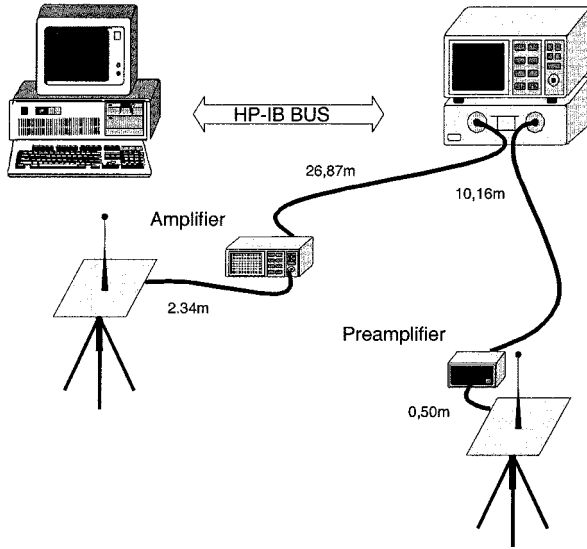


Fig. 1. UHF measurement system.

TABLE I
SLL AND rms DELAY SPREAD OF
DIFFERENT WINDOWS

WINDOW	SLL [dB]	$(\tau_{\text{rms}})_{\text{window}}$ [ns]
Rectangular	-13	$\sim 10^9$
Hanning	-42	1.02
Kaiser-Bessel (window parameter=3)	-70	1.22
Blackman-Harris	-92	1.36

The shape of the window used in the frequency measurements affects the IRs as follows:

$$h(\tau, t)_{\text{estimated}} = h(\tau, t)_{\text{channel}} * h_{\text{window}}(\tau). \quad (4)$$

As a result, the impulse response is averaged and the delay resolution is reduced. Four different windows were considered in this study: rectangular, Hanning, Blackman–Harris, and Kaiser–Bessel. The side-lobe levels (SLLs) for these windows are given in Table I. The lower the SLL, the wider the main window lobe becomes [9]. A wider main lobe yields a lower delay resolution in the IR.

If the channel satisfies the wide sense stationary uncorrelated scattering (WSSUS) assumption, the power delay profile (PDP) is given by

$$P_h(\tau) = \langle |h(\tau, t)|^2 \rangle. \quad (5)$$

Wide-band parameters, as the mean delay τ_{mean} , the rms delay spread τ_{rms} , and the coherence bandwidth at level $c \in [0, 1]$, B_c are calculated. The mean delay τ_{mean} is the average of the delays of all paths

$$\tau_{\text{mean}} = \frac{\int_0^{\tau_{\text{max}}} \tau P_h(\tau) d\tau}{\int_0^{\tau_{\text{max}}} P_h(\tau) d\tau}. \quad (6)$$

The radio channel time dispersion is characterized by the rms delay spread τ_{rms} , calculated as

$$\tau_{\text{rms}} = \sqrt{\frac{\int_0^{\tau_{\text{max}}} (\tau - \tau_{\text{mean}})^2 P_h(\tau) d\tau}{\int_0^{\tau_{\text{max}}} P_h(\tau) d\tau}}. \quad (7)$$

From (4), it can be demonstrated [10] that the channel delay spread is overestimated, the increase being due to the window shape

$$(\tau_{\text{rms}})_{\text{estimated}}^2 = (\tau_{\text{rms}})_{\text{channel}}^2 + (\tau_{\text{rms}})_{\text{window}}^2 \quad (8)$$

where $(\tau_{\text{rms}})_{\text{window}}$ is the delay spread corresponding to the window impulse response. Values of $(\tau_{\text{rms}})_{\text{window}}$ for the four different windows considered in this work have been calculated and are presented in Table I.

The frequency correlation function of the radio channel can be obtained from the PDP as

$$R_T(\Delta f) = \int_{-\infty}^{\infty} P_h(\tau) e^{-j2\pi\Delta f\tau} d\tau. \quad (9)$$

For a particular correlation level c , typically 0.9, 0.7, or 0.5, B_c is the minimum frequency separation for which the norm of the frequency correlation function crosses this level. As an example, $B_{0.5}$ is calculated as

$$B_{0.5} = \min(\Delta f) \text{ such that } |R_T(\Delta f)| = 0.5. \quad (10)$$

For low values of c , this parameter represents the minimum frequency separation to have the components of the radio signal sufficiently uncorrelated.

III. ENVIRONMENT DESCRIPTION

Measurements were carried out in three different environments: a computer laboratory with rows of PC desks; an electronics laboratory with electronic equipments such as oscilloscopes, signal generators, and synthesizers on benches; and a corridor. The plan of these environments, with the dimensions in centimeters, is given in Fig. 2. In each environment, the receiver antenna was shifted to various positions separated one-eighth of a wavelength along a line. A total of 260, 240, and 50 different positions were used in the corridor, the computer laboratory, and the electronics laboratory, respectively. The transmitter and receiver antenna positions are also shown in Fig. 2. As can be seen, the LoS condition is always satisfied.

IV. IMPACT OF WINDOWING ON THE ESTIMATED POWER DELAY PROFILES AND DELAY SPREADS

Despite the fact that the measurement system averages the results of several frequency sweeps to reduce the noise in the measurement, the frequency response and the IR will be corrupted by noise. Generally, a noise threshold is applied to raw IRs in order to separate actual multipath components from noise. Several methods to calculate this threshold noise can be found in

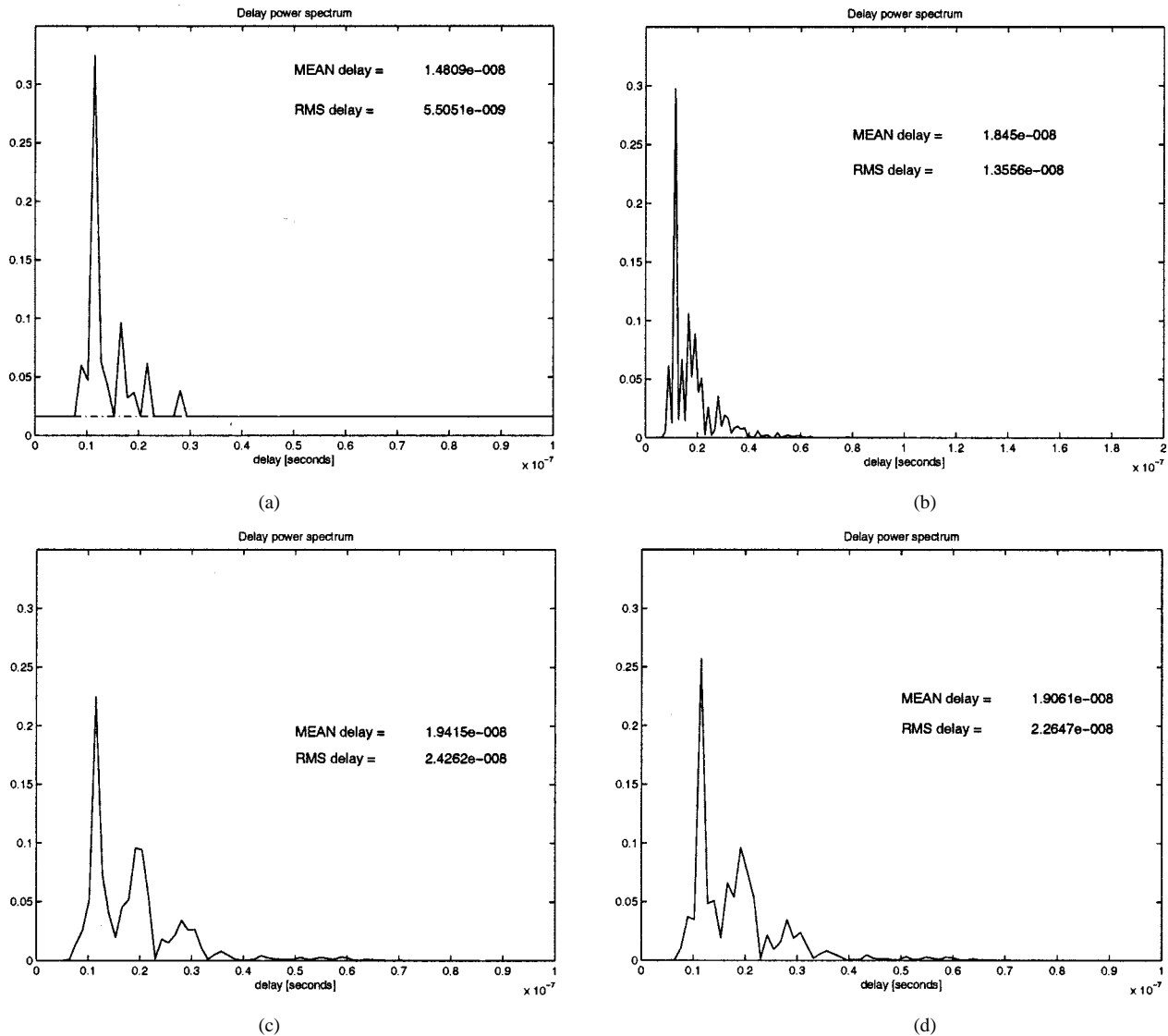


Fig. 3. PDPs obtained in a corridor for various selected windows. (a) Rectangular window, (b) Hanning, (c) Blackman-Harris, and (d) Kaiser-Bessel ($\alpha = 3$).

actual noise level but on the frequency window used for the measurements. The noise threshold estimation is improved by the proposed method because it combines the limits given by the actual noise power and the limit imposed by the window SLL.

To illustrate the effect of the frequency windowing on the IRs, the PDPs and the delay parameters have been calculated, with different frequency windows, at a fixed position in the corridor. They are shown in Fig. 3. The τ_{rms} values range from 5.5 to 24.3 ns, depending on the window used. In view of the values of $(\tau_{\text{rms}})_{\text{window}}$ of Table I, the large variation of the delay spread cannot be completely explained by the only effect described in (8).

In order to gain a better understanding of the window effect on the delay spread, the threshold used to distinguish signal from noise in the PDPs has to be studied. When the rectangular window is used ($\text{SSL} = -13$ dB), the overall threshold is fixed by the window SLL, because the two other levels are much lower. In this case, due to the high value of the threshold, some low-power multipath components are not considered and τ_{rms}

is underestimated. The other windows present lower SLLs, so the threshold is given by the actual noise level. For these cases, a larger number of multipath components are taken into account in the calculation and a better estimation of the delay spread is obtained. In general, lower window SLLs yield larger values of τ_{rms} . In terms of signal delay dispersion, this means that a larger value is obtained when windows such as Blackman-Harris are used.

V. RMS DELAY AND MEAN DELAY

The dependence of the rms delay on the mean delay has been analyzed in the three different environments described in Section III for copolar (vertical-vertical) and crosspolar (vertical-horizontal) components.

From the measurements collected in the three environments, τ_{mean} and τ_{rms} have been estimated. They are plotted in Figs. 4, 7, and 9 as a function of the separation between antennas. The values obtained are comparable to those found in the literature for indoor environments [10], [12], [15], [16]. The mean delay

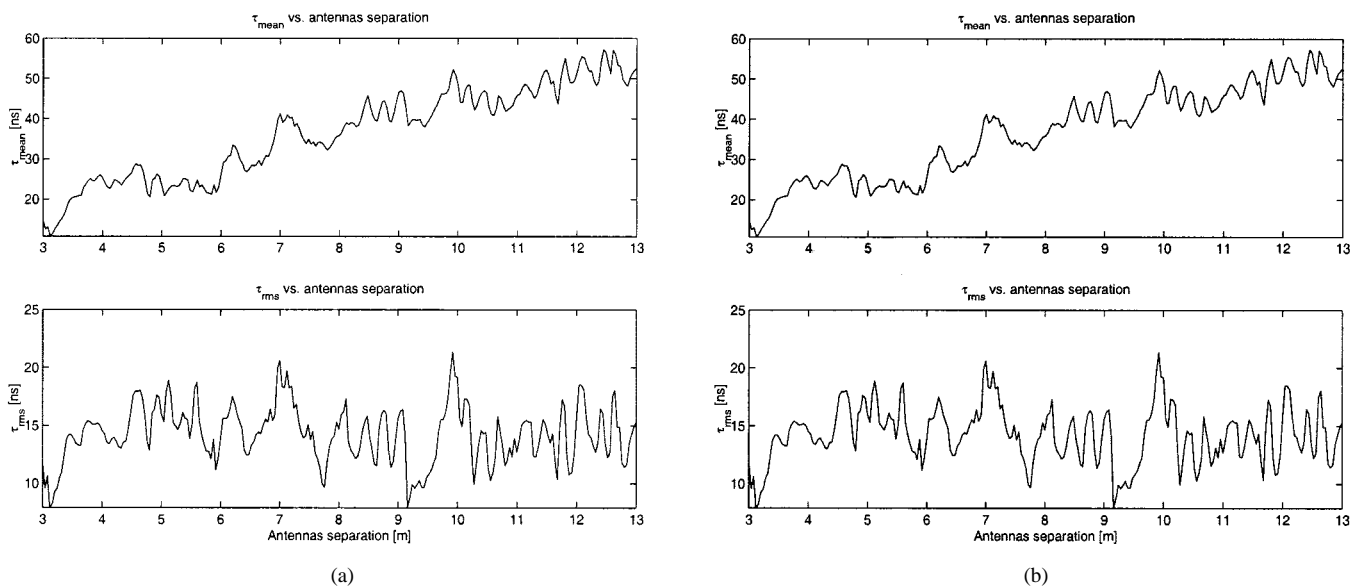


Fig. 4. Mean delay and rms delay versus transmitter–receiver separation in the corridor. (a) Copolar and (b) crosspolar component.

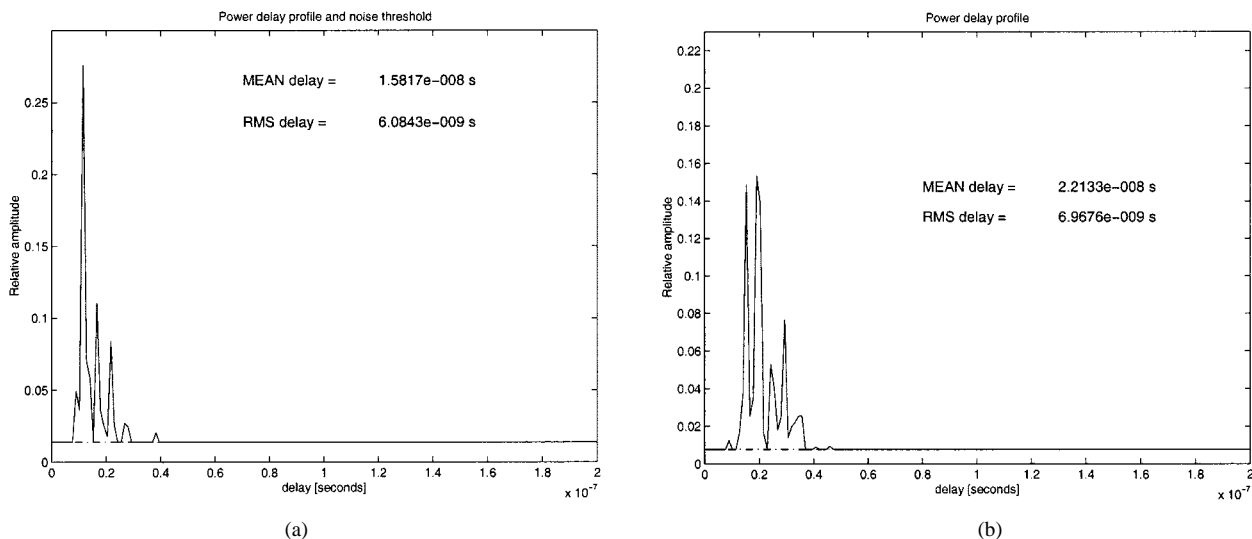


Fig. 5. PDP in the corridor. (a) Copolar and (b) crosspolar component.

exhibits a trend to increase with distance. Some authors have reported that rms delay spread increases with antenna separation [15]. However, the rms delay spread is almost constant in the plots presented in this paper because of the short receiver antenna path. As the transmitter antenna is moved away from the receiver antenna, the amplitudes of the reflected signals relative to the direct path become larger, and this produces the increase of the mean and rms delays. However, due to the limited delay resolution of the measurement system, some oscillations are superimposed to the trend described above. After a thorough analysis of the IRs, it has been found that contributions with close delays cannot be resolved and interfere, giving rise both to a fast spatial variation of some IR and PDP components and to the oscillation of the delay parameters with the distance between antennas. It should be noted that no averaging of several squared envelopes of the impulse responses is performed because the effect of fast variation is also an issue of study. This explains the fluctuations that the estimated mean delays and rms

delay spreads exhibit as the separation between the transmitter and the receiver is changed.

Values of both parameters are lower for the copolar than for the crosspolar component because the copolar IRs present a dominant ray while the crosspolar ones do not. To illustrate these differences, a sample of the IRs corresponding to both components is presented in Fig. 5. This difference can be quantified by calculating the K factor, which represents the ratio between the power of the direct ray to the power of the reflected components. The mean value of the K factor along the corridor is 0.32 for the copolar measurements and 0.23 for the crosspolar ones, so the relative contribution of the direct component is more significant in the copolar IR.

The linear dependency between both delay parameters can be measured by their correlation coefficients. These have been calculated and are listed in Table II. The high correlation values suggest that a linear relation in the form $\tau_{\text{rms}}[\text{ns}] = a\tau_{\text{mean}}[\text{ns}] - b$ can model the dependence between

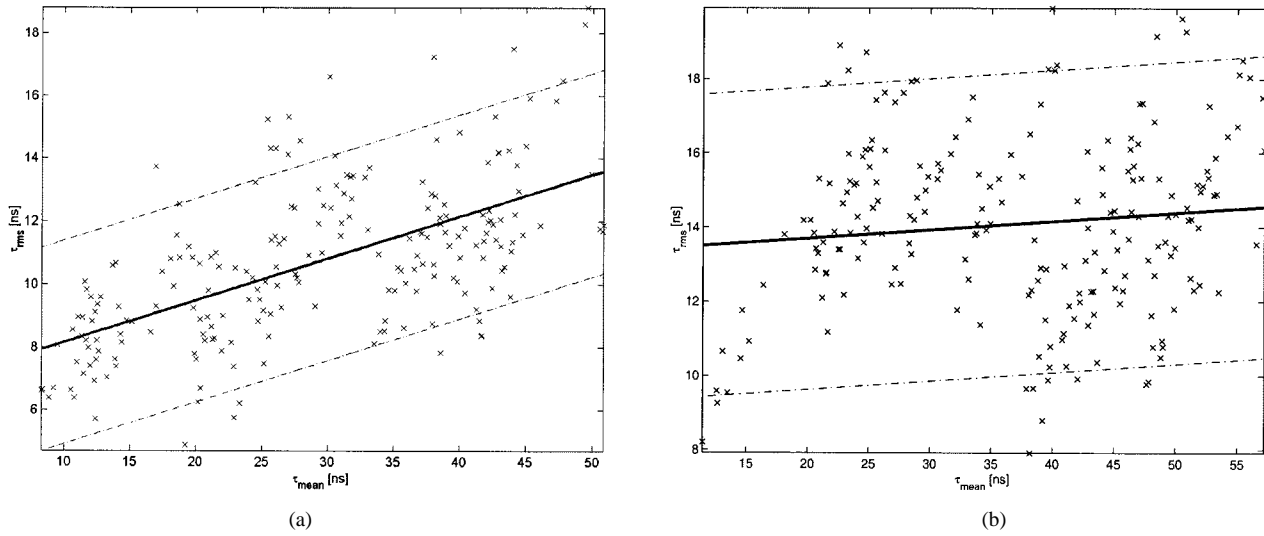


Fig. 6. RMS delay versus mean delay in the corridor: measured data, linear fit, and 90% confidence interval. (a) Copolar and (b) crosspolar component.

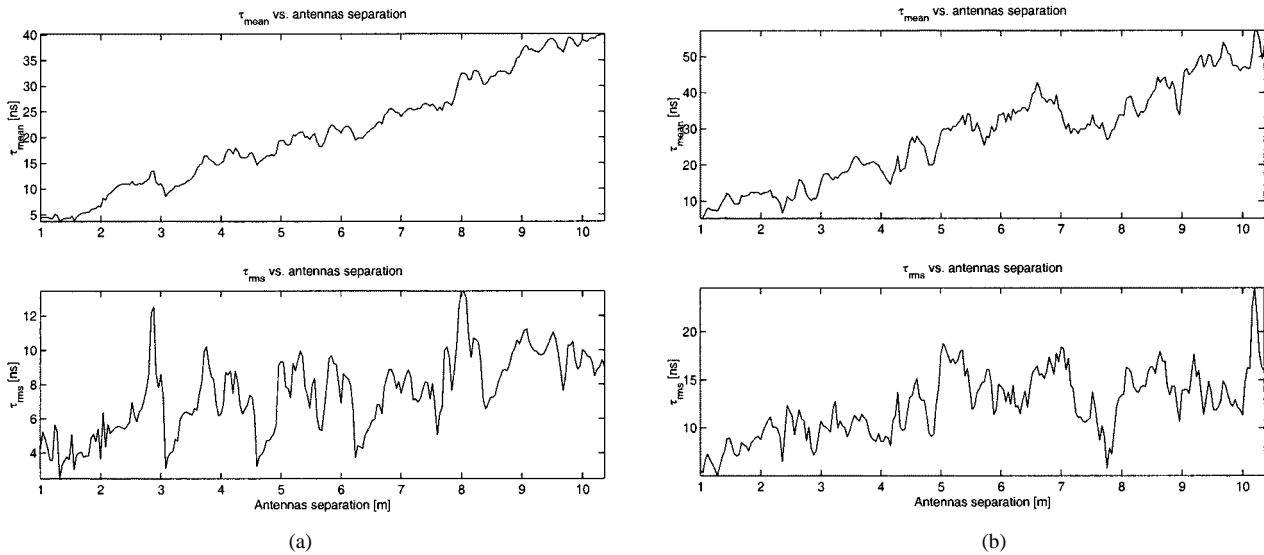


Fig. 7. Mean delay and rms delay versus transmitter-receiver separation in the PC laboratory. (a) Copolar and (b) crosspolar component.

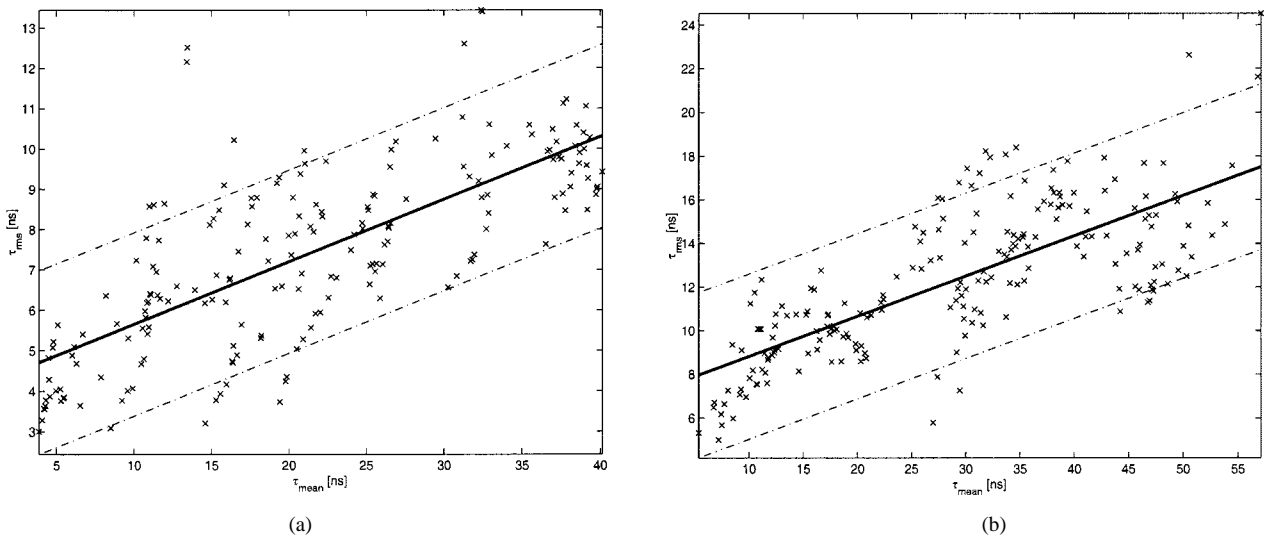


Fig. 8. Rms delay versus mean delay in the PC laboratory: measured data, linear fit, and 90% confidence interval. (a) Copolar and (b) crosspolar component.

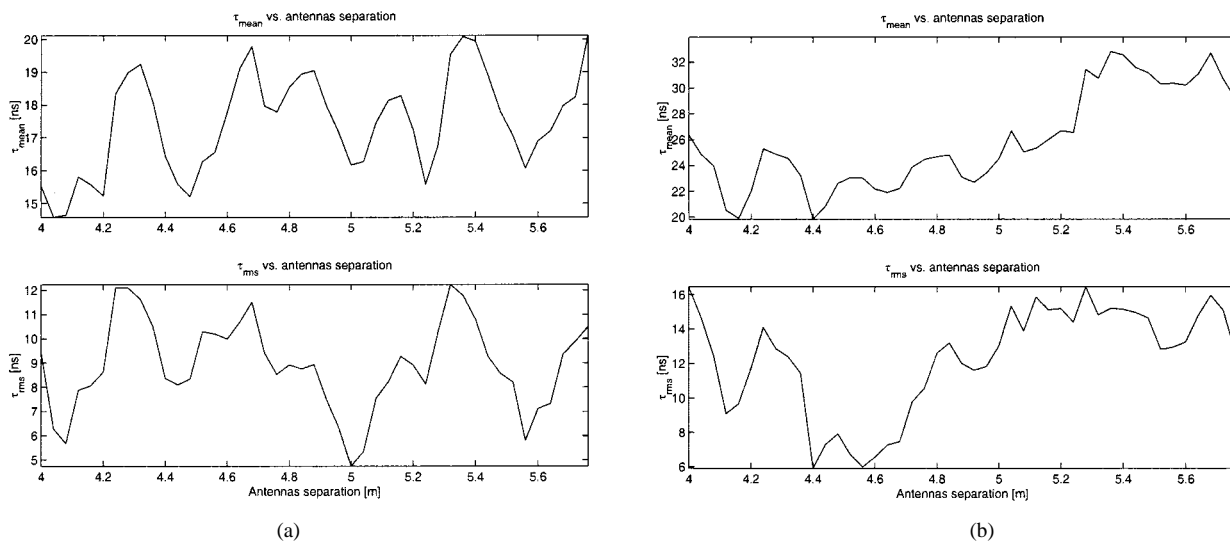


Fig. 9. Mean delay and rms delay versus transmitter–receiver separation in the electronics laboratory. (a) Copolar and (b) crosspolar component.

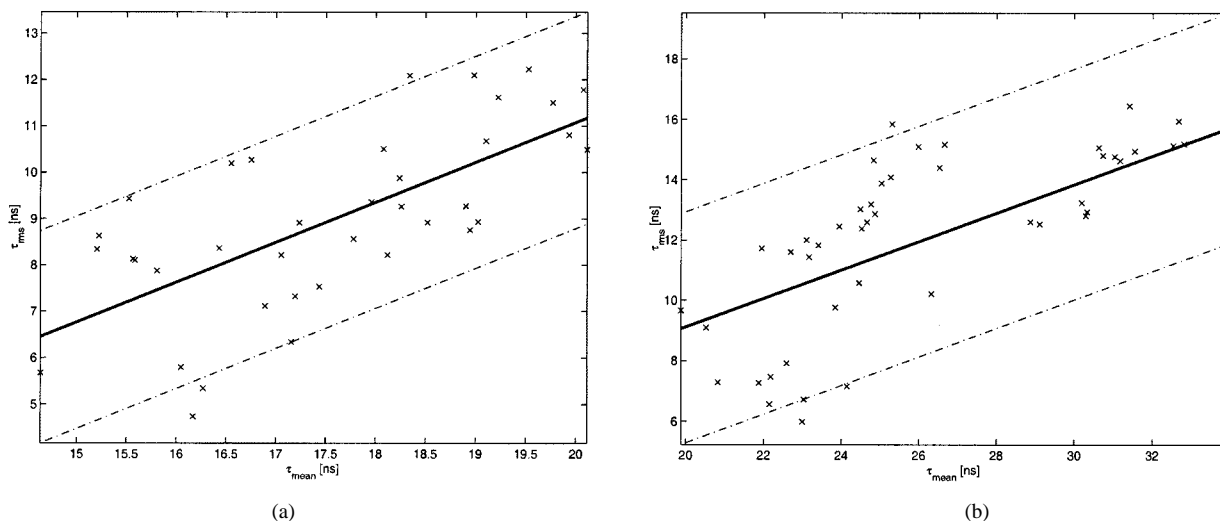


Fig. 10. RMS delay versus mean delay in the electronics laboratory: measured data, linear fit, and 90% confidence interval. (a) Copolar (b) and crosspolar component.

TABLE II
a AND *b* PARAMETERS, CORRELATION FACTOR, CONFIDENCE INTERVAL, AND LMS ERROR FROM THE τ_{RMS} VERSUS τ_{MEAN} LINEAR FIT

Component	CORRIDOR		PC LABORATORY		ELECTRONICS LABORATORY	
	Copolar	Crosspolar	Copolar	Crosspolar	Copolar	Crosspolar
Correlation factor	0.58	0.15	0.74	0.73	0.67	0.63
<i>a</i>	0.13	0.03	0.15	0.18	0.88	0.47
<i>b</i> (ns)	-6.82	-13.05	-4.11	-6.97	19.68	0.35
90% confidence interval (ns)	± 3.23	± 4.17	± 2.27	± 3.78	± 2.29	± 3.82
LMS error	0.182	0.175	0.199	0.176	0.152	0.186

τ_{mean} and τ_{RMS} . The results of a linear fit to the measured data are presented in Figs. 6, 8, and 10 and in Table II, including the values of parameters *a* and *b*, the confidence interval for 90% of the data, and the LMS error of the fit. The goodness of the linear fit has been confirmed by a Kolmogorov–Smirnov test [17], which shows that the residuals follow a Gaussian distribution.

For the three environments considered, it has been found that τ_{mean} and τ_{RMS} are high correlated. It should be noted that both parameters are calculated from the same impulse response and that both may have a dependence on a third common variable that is the Tx–Rx separation. Again, the presence of a dominant component in the copolar IRs makes the linear dependence stronger for this component than for the crosspolar one.

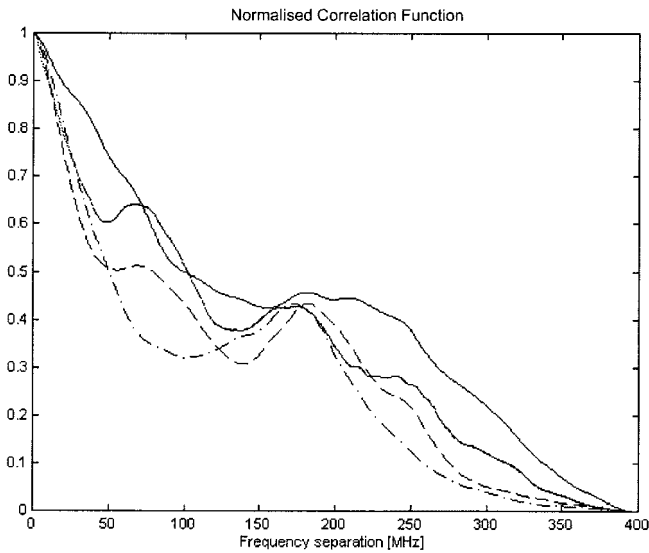


Fig. 11. Frequency correlation function at four different measurement points. Copolar component.

VI. DELAY SPREAD AND COHERENCE BANDWIDTH

The frequency correlation function is shown in Fig. 11 at four different positions along the corridor. As expected [2], [3], the correlation decreases when increasing the frequency separation and, due to the limited frequency band of the measurement, falls to zero for a separation of 392 MHz. It can also be seen that the decrease is not monotonous because the presence of significant multipath in the radio channel produces an oscillation on the general trend of the curve [2], [4], [18].

Once the correlation function is obtained and a correlation level c is given, B_c can be estimated. At each antenna position along the corridor, the coherence bandwidth for a correlation level of 0.9 has been calculated. The results are plotted as a function of the antennas separation in Fig. 12 for copolar and crosspolar components. The coherence bandwidth is larger for the copolar component. This is consistent with the τ_{rms} results and the inverse relation between these two parameters. As happens with the rms delay spread, some oscillations are superimposed to the mean coherence bandwidth. It was explained before that these oscillations are caused by the multipath propagation and the absence of a spatial averaging.

The relation between B_c and τ_{rms} has been long investigated. As a result of some experimental studies, Gans [19] proposed a relation of the form $B_c = 1/(\alpha \cdot \tau_{\text{rms}})$, where α ranged from six to ten depending on the shape of the PDP. In Jakes [2], as a result of a theoretical analysis of exponentially decaying power delay profiles, a value of $\alpha = 2\pi$ was found. The inverse model is also proposed in [7], with $\alpha = 1/0.15$. In [16], for an indoor channel, it was found that α could vary between small values and ten. Also in [16], larger values of α are observed in obstructed situations than in LoS situations. A study based on a two-ray model of the impulse response [18] supports the model $B_c = 1/(\alpha \cdot \tau_{\text{rms}})$, with a value of $\alpha = 6$. Other models used to characterize the relation between τ_{rms} and B_c can be found in [6], where, based on the results of a measurement campaign, a relation of the form $B_c = C\tau_{\text{rms}}^{-\beta}$ is used, or in [5], where a lower bound of the form $B_c \geq (2\pi\tau_{\text{rms}})^{-1} \arccos(c)$ is derived.

B_c values depicted in Fig. 12 have been compared to τ_{rms} values plotted in Fig. 4. This is done in Fig. 13, where the pairs (τ_{rms}, B_c) measured at each position in the corridor have been plotted. Plots of the pairs (τ_{rms}, B_c) obtained in the PC laboratory and in the electronics laboratory are presented in Figs. 14 and 15.

A relation of the form $B_c = C\tau_{\text{rms}}^{-\beta}$, where B_c is expressed in [MHz] and τ_{rms} in [ns] [6], has been considered. In order to fit the curve $B_c = C\tau_{\text{rms}}^{-\beta}$, a log-log transformation of the pairs (τ_{rms}, B_c) is performed so the relation becomes linear. Then a regression line is fitted to the scatter plot of pairs $(\ln(\tau_{\text{rms}}), \ln(B_c))$. The results of the fit are given in Table III and Figs. 13–15.

The lower bound for B_c given in [5] has been reported in Figs. 13–15 for comparison purposes. It is observed that most of the pairs $(\tau_{\text{rms}}, B_{0.9})$ are located above this curve. However, for shorter values of τ_{rms} , there are some pairs below the lower bound. Lower values of τ_{rms} correspond to shorter separations between antennas. In this situation, the mean signal value changes rapidly and the wide-sense-stationary property assumed in [5] for the lower bound calculation is not verified.

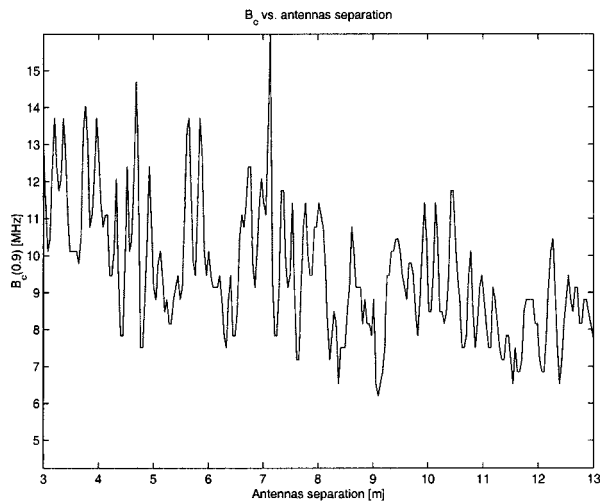
The values for C and β , are lower than those found in [6], where a different frequency band (900–1100 MHz) and correlation level (0.5) have been considered. In the corridor and in the PC laboratory, values of β are around 0.5 for the copolar component and around 0.6 for the crosspolar one. In the electronics laboratory, shorter values of β have been obtained. Due to the dependence of τ_{rms} and B_c on the IR shape, the crosspolar component presents a larger decaying slope than the copolar one.

VII. CONCLUSION

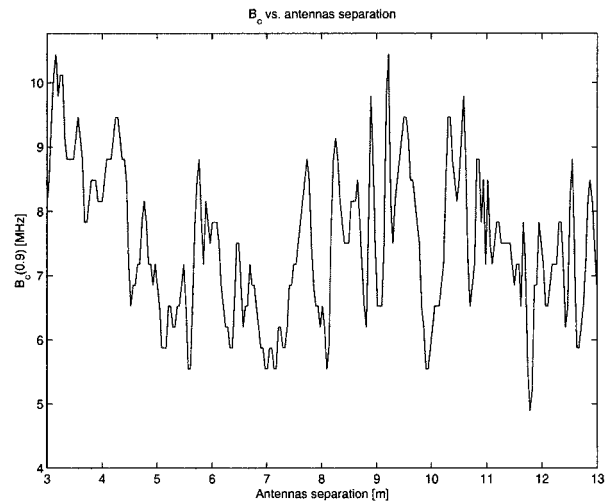
The radio channel has been investigated in the 470–862 MHz band in three different indoor environments. A combined method is presented in order to filter noise from the frequency response. With this method, more accurate estimations of τ_{mean} and τ_{rms} can be calculated. The effect of four different frequency windows on the results has been analyzed. In general, windows with lower SLLs lead to larger values of τ_{mean} and τ_{rms} . The Blackman–Harris window yields more accurate estimations and larger values of the delay parameters than other windows.

The variation of τ_{mean} and τ_{rms} with the antennas separation has been presented. As the receiver antenna is separated from the transmitter antenna, the amplitudes of the reflected signal relative to the direct path become larger, which results in the increase of τ_{mean} and τ_{rms} . Due to the fact that the copolar component contains the stronger contribution of the LoS wave, the values of τ_{mean} and τ_{rms} are lower for the copolar than for the crosspolar component.

It has been demonstrated for the three environments that both parameters exhibit a high correlation and a linear dependence. In all the cases, the correlation and the linear dependence are higher for the copolar than for the crosspolar component. The correlation is also higher in the laboratories than in the corridor. The linear fits have positive slopes that vary with the environment and the polarization component considered.

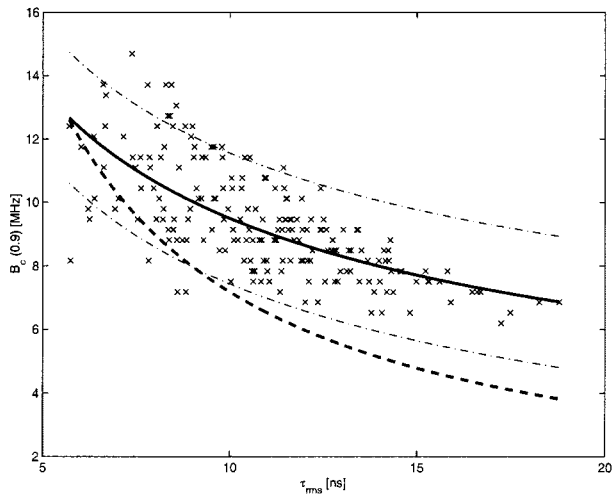


(a)

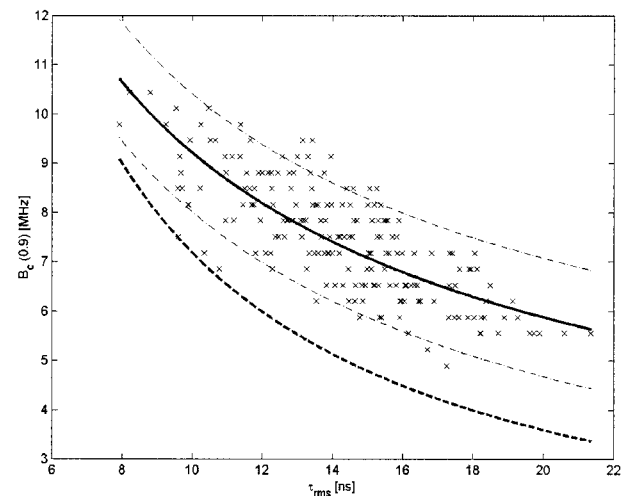


(b)

Fig. 12. $B_c(0.9)$ in the corridor. (a) Copolar and (b) crosspolar component.

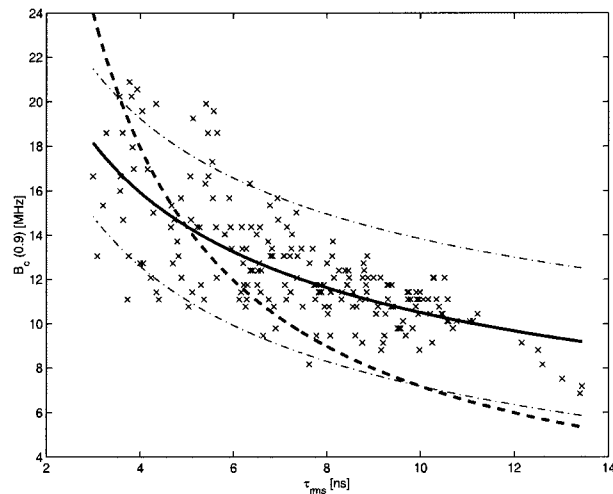


(a)

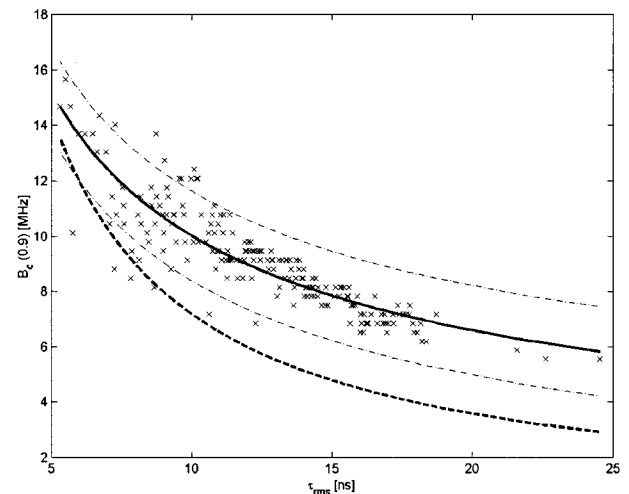


(b)

Fig. 13. Coherence bandwidth at level 0.9 versus the separation between the transmitter and the receiver in the corridor. (a) Copolar and (b) crosspolar component.



(a)



(b)

Fig. 14. Coherence bandwidth at level 0.9 versus the separation between the transmitter and the receiver in the PC laboratory. (a) Copolar and (b) crosspolar component.

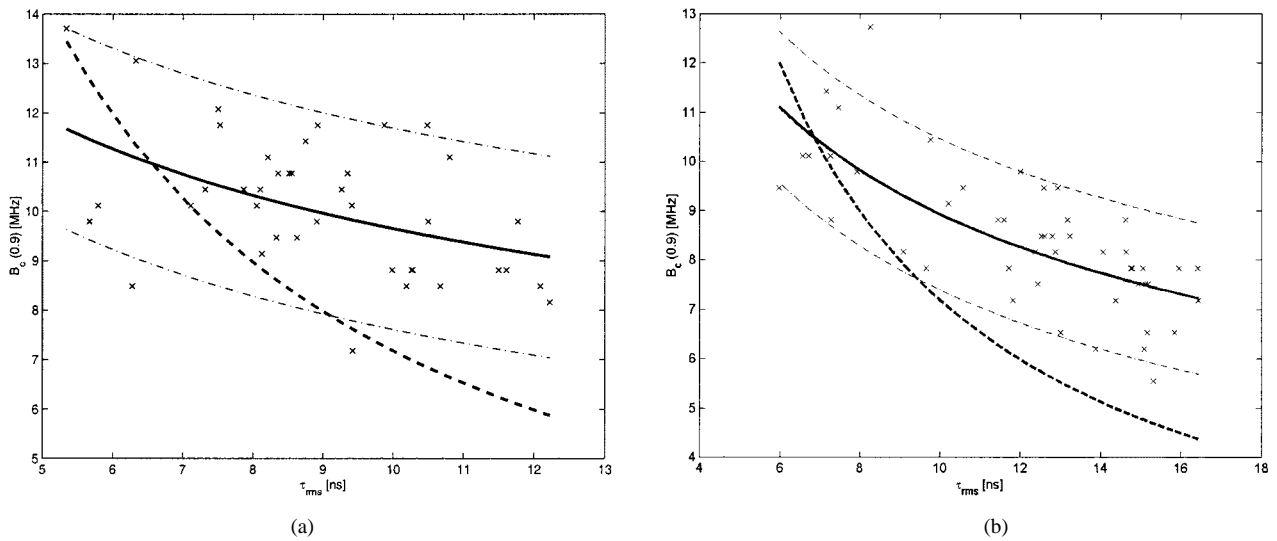


Fig. 15. Coherence bandwidth at level 0.9 versus the separation between the transmitter and the receiver in the electronics laboratory. (a) Copolar and (b) crosspolar component.

TABLE III
PARAMETERS C AND β , CONFIDENCE INTERVAL, AND LMS ERROR FROM THE B_c VERSUS τ_{rms} FIT

Component	CORRIDOR		PC LABORATORY		ELECTRONICS LABORATORY	
	Copolar	Crosspolar	Copolar	Crosspolar	Copolar	Crosspolar
C	30.92	40.88	29.87	39.97	19.38	23.81
β	0.51	0.64	0.45	0.60	0.30	0.43
90% confidence interval (MHz)	± 2.06	± 1.19	± 3.32	± 1.62	± 2.04	± 1.53
LMS error	0.133	0.099	0.148	0.101	0.119	0.115

The coherence bandwidth for a correlation level of 0.9 has been calculated for each of the antenna positions along the corridor. It has been confirmed that an inverse relation between B_c and τ_{rms} exists. The results of the fit of the relation with the form $B_c = C\tau_{\text{rms}}^{-\beta}$ are presented. Measurements are also compared with the lower bound given in [5]. The differences in the results for both polarization components are due to the different shape of the IRs.

REFERENCES

- [1] J. G. Proakis, *Digital Communications*, 2nd ed. New York: McGraw-Hill, 1989.
- [2] W. C. Jakes, *Microwave Mobile Communications*. New York: Wiley, 1974.
- [3] W. C. Y. Lee, *Mobile Communications Design Fundamentals*, 2nd ed. New York: Wiley, 1993.
- [4] D. C. Cox and R. P. Leck, "Correlation bandwidth and delay spread multipath propagation statistics for 910-MHz urban mobile radio channels," *IEEE Trans. Commun.*, vol. COM-23, pp. 1271–1280, Nov. 1975.
- [5] B. H. Fleury, "An uncertainly relation for WSS processes and its application to WSSUS systems," *IEEE Trans. Commun.*, vol. 44, pp. 1632–1634, Dec. 1996.
- [6] S. J. Howard and K. Pahlavan, "Measurement and analyzes of the indoor radio channel in the frequency domain," *IEEE Trans. Instrum. Measure.*, vol. 39, pp. 751–755, Oct. 1990.
- [7] K. Pahlavan and S. J. Howard, "Frequency domain measurements of indoor radio channels," *Electron. Lett.*, vol. 25, no. 24, pp. 1645–1647, Nov. 1989.
- [8] P. A. Bello, "Characterization of randomly time-variant linear channels," *IEEE Trans. Commun. Syst.*, vol. CS-11, pp. 360–393, Dec. 1963.
- [9] M. C. Jeruchim, P. Balaban, and K. S. Shanmugan, *Simulation of Communications Systems*. New York: Plenum, 1992.
- [10] A. A. M. Saleh and R. A. Valenzuela, "A statistical model for indoor multipath propagation," *IEEE J. Select. Areas Commun.*, vol. SAC-5, pp. 128–137, Feb. 1987.
- [11] T. S. Rappaport and S. Y. Seidel, "900 MHz multipath propagation measurements for U.S. digital cellular radiotelephone," *IEEE Trans. Veh. Technol.*, vol. 39, pp. 132–139, May 1990.
- [12] P. Nobles and F. Halsall, "Delay spread measurements within a building at 2 GHz, 5 GHz and 17 GHz," in *Proc. Inst. Elect. Eng. Colloq. Propagation Aspects of Future Mobile Systems*, Oct. 1996, pp. 8/1–8/6.
- [13] S.-C. Kim, H. L. Bertoni, and M. Stern, "Pulse propagation characteristics at 2.4 GHz inside buildings," *IEEE Trans. Veh. Technol.*, vol. 45, pp. 579–592, Aug. 1996.
- [14] Probability distributions used in the radioelectric waves propagation, in Inform 1007–1 of the ITU, 1986–1990.
- [15] T. A. Sexton and K. Pahlavan, "Channel modeling and adaptative equalization of indoor radio channels," *IEEE J. Select. Areas Commun.*, vol. 7, pp. 114–121, Jan. 1989.
- [16] G. J. M. Janssen, P. A. Stigter, and R. Prasad, "Wideband indoor channel measurements and BER analysis of frequency selective multipath channels at 2.4, 4.75, and 11.5 GHz," *IEEE Trans. Commun.*, vol. 44, pp. 1272–1288, Oct. 1996.
- [17] D. P. S. de Rivera, *Estadística. Modelos y métodos: Modelos lineales y series temporales*, 2nd ed. Madrid, Spain: Alianza Editorial, 1989, vol. 2.
- [18] M. P. Fitton, A. R. Nix, and M. A. Beach, "A comparison of RMS delay spread and coherence bandwidth for characterization of wideband channels," in *Proc. Inst. Elect. Eng. Colloq. Propagation Aspects of Future Mobile Systems*, Oct. 1996.
- [19] M. J. Gans, "A power-spectral theory of propagation in the mobile-radio environment," *IEEE Trans. Veh. Technol.*, vol. VT-21, pp. 27–37, Feb. 1972.



Mercedes Sánchez Varela was born in Vigo, Spain, in 1974. She received the M.S. degree in telecommunications engineering from the Universidade de Vigo in 1998, where she is currently pursuing the Ph.D. degree in the Departamento de Tecnoloxías das Comunicacións.

During 2000, she was a Visiting Researcher at the Department of Engineering Science, University of Oxford, U.K. Her research interests include radio channel characterization and measurement. She has performed measurement campaigns with a vector network analyzer and now is processing results. She is also working on antenna analysis and design for DVB-T distribution networks.



Manuel García Sánchez (S'88–M'93) received the Ingeniero de Telecomunicación degree from the Universidad de Santiago de Compostela, Spain, in 1990 and the Doctor Ingeniero de Telecomunicación degree from the Universidad de Vigo, Spain, in 1996.

In 1990, he joined the Departamento de Tecnologías de las Comunicaciones, Universidad de Vigo, where he currently teaches courses in electromagnetic fields as a Profesor Titular de Universidad. He has been a Visiting Researcher at the Departamento de Señales, Sistemas y Radiocomunicaciones, Universidad Politécnica de Madrid, Spain, and the Department of Electronics and Information Technology, University of Glamorgan, U.K. His research interests include studies of indoor and outdoor radio channel modeling for wide-band applications at millimeter-wave frequencies, mobile communications, and DVB-T distribution networks.